

# Potential energy landscape and finite-state models of array-enhanced stochastic resonance

John F. Lindner,<sup>1</sup> Matthew Bennett,<sup>2</sup> and Kurt Wiesenfeld<sup>2</sup>

<sup>1</sup>Physics Department, The College of Wooster, Wooster, Ohio 44691, USA

<sup>2</sup>Center for Nonlinear Science and School of Physics, Georgia Institute of Technology, Atlanta, Georgia 30332, USA

(Received 28 November 2005; published 9 March 2006)

Noise and coupling can optimize the response of arrays of nonlinear elements to periodic signals. We analyze such array-enhanced stochastic resonance (AESR) using finite-state transition rate models. We simply derive the transition rate matrices from the underlying potential energy function of the corresponding Langevin problem. Our implementation exploits Floquet theory and provides useful theoretical and numerical tools. Our framework both facilitates analysis and elucidates the mechanism of AESR. In particular, we show how sublinear coupling diminishes AESR, but superlinear coupling enhances it.

DOI: [10.1103/PhysRevE.73.031107](https://doi.org/10.1103/PhysRevE.73.031107)

PACS number(s): 05.40.-a, 02.50.-r

## I. INTRODUCTION

Twenty-five years ago, Benzi *et al.* [1] introduced the phenomenon of stochastic resonance (SR), a noise-enhanced response to weak signal. An early application was a possible mechanism for climatic change. Since then, this nonlinear phenomenon has been studied extensively and generalized in many ways [2]. An important extension includes related phenomena in coupled systems. Jung *et al.* [3] proved that global coupling could enhance the spectral power amplification of the collective, summed response of an array of stochastic resonators. Lindner *et al.* [4] demonstrated numerically that local coupling could enhance the signal-to-noise ratio (SNR) of individual stochastic resonators, and that this array-enhanced stochastic resonance (AESR) was accompanied by spatiotemporal synchronization for an optimal coupling and noise whose strength and intensity scaled simply with array size [5]. Marchesoni *et al.* [6] derived these scaling laws analytically by mapping the discrete problem onto the kink-antikink dynamics of a continuous  $\phi^4$  model. More recently, Kanamaru *et al.* [7] derived similar scaling laws for AESR in a system of diffusively coupled FitzHugh-Nagumo model neurons, suggesting that this phenomenon may be important in naturally occurring neuronal and sensory arrays.

Löcher and collaborators [8] first realized AESR experimentally in arrays of diode resonators, and later [9] demonstrated AESR numerically in a coupled map lattice. Rowe and Etchegoin [10] then observed AESR and related phenomena in linearly coupled Schmitt triggers. Recently, Sharpe *et al.* [11] obtained similar results in two-dimensional arrays of liquid crystal light valves. The occurrence of AESR in coupled ordinary differential equations, coupled map lattices, a  $\phi^4$  model, and experimentally in diverse one- and two-dimensional systems suggests its universal nature.

Schimansky-Geier and colleagues [12–14] have studied AESR extensively. After obtaining analytic expressions for the SNR of the summed output of two (nonidentical) resonators in the limits of strong and weak coupling [12], they generalized the two-state transition rate model of SR to arrays of coupled stochastic resonators [15]. They chose a transition rate matrix so that the array evolved according to a solvable stochastic Ising model, thereby allowing them to demonstrate analytically that, in the weak-signal limit, cou-

pling can increase the SNR of individual elements but not the SNR of the collective, summed output of all the elements in the array [13,14].

We also seek to create finite-state transition rate models of AESR, simple prototype systems that facilitate analysis of coupling on stochastic resonance. To explicitly apply the rate theory one must choose a transition matrix. In this paper, we will describe a general and intuitive technique for constructing a transition rate matrix based on an underlying Langevin model, a set of stochastic differential equations in a potential energy landscape. Our implementation of the rate model will exploit the periodicity of the global forcing to yield numerical and analytic advantages. We find that these rate models compare favorably with the well-established Langevin models. Along the way, our heuristics will show how nonlinear coupling can enhance or suppress AESR.

## II. LANGEVIN MODEL

We first consider an overdamped chain of bistable oscillators with local, linear coupling subject to a global signal and local noise. Let the components  $x_n$  of the  $N$ -dimensional vector  $\vec{x}$  specify the state of the  $N$  oscillators. The evolution obeys the Langevin equation

$$\partial_t \vec{x} = -\vec{\nabla} U[\vec{x}, t] + \vec{\xi}[t], \quad (1)$$

where the time-dependent potential energy can be decomposed into three components

$$U[\vec{x}, t] = U_0[\vec{x}] + U_c[\vec{x}] + U_s[\vec{x}, t]. \quad (2)$$

The first component is the unperturbed, bistable energy

$$U_0[\vec{x}] = \sum_{i=1}^N \left( -\frac{1}{2} a x_i^2 + \frac{1}{4} b x_i^4 \right), \quad (3)$$

with barrier height  $h = a^2/4b$  and barrier half-width  $c = \sqrt{a/b}$ . The second component is the coupling energy

$$U_c[\vec{x}] = \sum_{i=1}^{N-1} \frac{1}{2} \kappa (x_i - x_{i+1})^2, \quad (4)$$

with coupling stiffness  $\kappa$ . The third component is the time-dependent signal energy

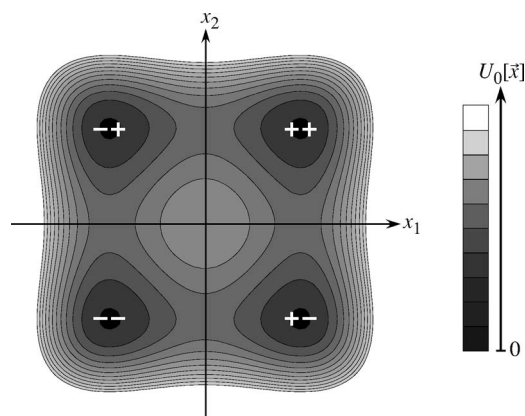


FIG. 1. Contour plot of unperturbed potential energy landscape  $U_0[\vec{x}]$ , for an array of  $N=2$  uncoupled and unforced oscillators, for parameters  $a=32$ ,  $b=1$ .

$$U_s[\vec{x}, t] = \sum_{i=1}^N \epsilon \cos(2\pi f t + \varphi) x_i, \quad (5)$$

with signal amplitude  $\epsilon$ , frequency  $f=1/T$ , and phase  $\varphi$ .

Ideally, the noise is Gaussian and white with zero mean

$$\langle \xi_i[t] \rangle = 0 \quad (6)$$

and  $\delta$  correlation

$$\langle \xi_i[t] \xi_j[t'] \rangle = 2D \delta_{ij} \delta(t - t'). \quad (7)$$

In practice, our computer simulations employ Gaussian band-limited white noise. Typical parameter values [15] are  $a=32$ ,  $b=1$  for the bistable potential wells, and  $\epsilon=8$ ,  $f=0.195$  for the signal.

Figure 1 is a contour plot of the unperturbed potential energy landscape  $U_0[\vec{x}]$ , which involves zero coupling and no signal ( $\kappa=\epsilon=0$ ), for  $N=2$  oscillators. There are four minima and nine extrema. The minima are labeled by the 2-tuples  $\{++, --, +-, --\}$  for future reference. (In general, there are  $2^N$  minima and  $3^N$  extrema, and the former are labeled by the corresponding  $N$ -tuples.)

Figure 2 shows the evolution of the potential energy with time and coupling, again for  $N=2$  oscillators. The global signal rocks the potential energy back and forth along the main diagonal. The potential minima invite us to consider transition rates among them.

We numerically integrate the stochastic Eq. (1) using the Euler-Maruyama algorithm [16] with a typical integration time step  $dt=T/2048 \approx 0.0025$ . We spectral analyze the numerically generated binary-filtered time series  $\text{sgn}[x_m(t)]$  of one of the middle oscillators with a temporal sampling of  $\Delta t$  and a frequency resolution of  $\Delta f$ . We Welch window the time series to reduce bin leakage, average at least 256 spectra, and find a sharp peak with power  $S$  superimposed on a Lorentzian background with interpolated power  $\mathcal{N}$  in the signal frequency bin. We compute the signal-to-noise ratio  $R = \Delta f(S/\mathcal{N} - 1)/G \geq 0$ , where the processing gain  $G=5/6$  accounts for the Welch window scaling of narrowband peaks. For the shortest array of  $N=2$ , Fig. 3 plots signal-to-noise ratio  $R$  versus noise intensity  $D$  for various coupling strengths  $\kappa$ . As coupling increases, the maximum  $R$  increases and then decreases, generating a maximum within a maximum, a hallmark of AESR.

### III. AESR HEURISTICS

Why does coupling enhance the SR? Consider transition rates among the minima of Fig. 2. Optimal coupling and noise will cause the state point to hop between the symmetric  $++$  and  $--$  wells synchronously with the signal. This does not happen for  $\kappa=0$  because there is a significant probability that the state point will be trapped in the asymmetric  $+-$  or  $-+$  wells, or that it will be trapped in the  $++$  or  $--$  well out of synchrony with the signal (for example, in the  $++$  well when it is highest rather than lowest). As  $\kappa$  increases, the  $+-$  and  $-+$  wells shrink until they disappear leaving level paths around the central maximum. These paths facilitate noise-enabled movement to the lowest of the symmetric  $++$  and  $--$  wells, and the SR is maximized. As  $\kappa$  increases further, these level paths shrink until they disappear leaving only the large central maximum as a barrier separating the

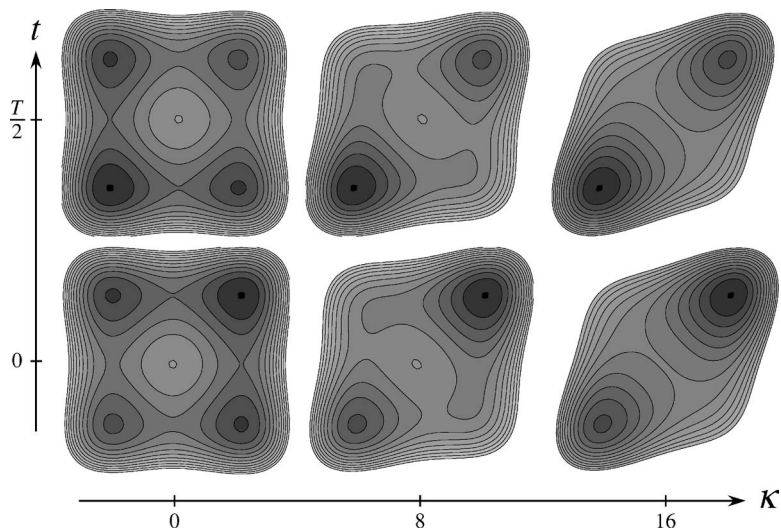


FIG. 2. Potential energy landscape  $U[\vec{x}, t]$  for different times  $t$  for an array of  $N=2$  oscillators, for different times  $t$  and coupling strengths  $\kappa$ . Parameters are  $a=32$ ,  $b=1$ , and  $\epsilon=8$ ;  $1/T=f=0.195$ .

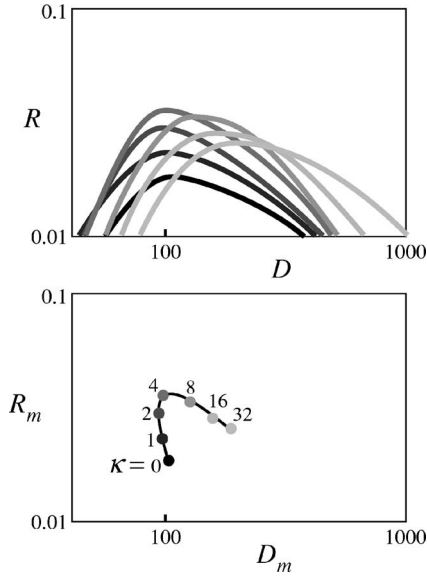


FIG. 3. Langevin AESR for  $N=2$ . Upper plot shows the signal-to-noise ratio  $R$  versus noise intensity  $D$  for different coupling strengths  $\kappa$ . Bottom plot focuses on movement of successive maxima, which reveals yet another maximum. Same parameters as in Fig. 2.

symmetric  $++$  and  $--$  wells. Synchronous hopping is now more difficult in this quasi-one-dimensional situation as the state point once again can get stuck in a well out of synchrony with the signal. This suggests that optimal coupling for  $N=2$  corresponds (at least roughly) to the vanishing of the asymmetric  $+ -$  and  $- +$  minima. Figure 4 depicts the movement of the potential energy extrema with coupling  $\kappa$ , including the destruction of half the minima, for  $N=2$ . Similar behavior obtains for larger  $N$ . One way to make this heuristic picture quantitative is to determine the relevant rates governing transitions between the various states. We now proceed to develop just such a rate description.

#### IV. RATE THEORY FORMULATION

Our starting point for a numerical rate formulation of AESR is the rate equation

$$\partial_t \vec{n}(t) = \mathbf{W}(t) \cdot \vec{n}(t), \quad (8)$$

where the  $\alpha$ th component of  $\vec{n}$  is the probability of finding the system in the state  $\alpha$  and  $\mathbf{W}$  is a  $T$ -periodic transition

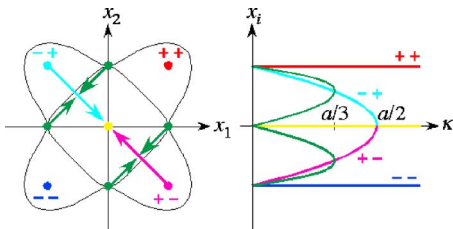


FIG. 4. (Color online) Potential energy extrema as a function of coupling  $\kappa$  for  $N=2$ . Asymmetric wells  $+ -$  and  $- +$  disappear when pinned between adjacent saddles. Same parameters as in Fig. 2.

matrix. We denote by  $S$  the total number of states. Of particular interest to us is a situation which closely reflects the  $N$  coupled double-well problem; however, before specializing we develop a general expression for the correlation function which exploits the inherent structure of Eq. (8).

#### A. Floquet representation of correlation function

If  $f(t)$  is a state function, then

$$\langle f[t_1]f[t_2] \rangle = \sum_{\alpha} \sum_{\beta} f_{\alpha} f_{\beta} P_c[\beta, t_2 | \alpha, t_1] P_{eq}[\alpha, t_1], \quad (9)$$

where the angular brackets denote an ensemble average. The conditional probabilities  $P_c$  and the equilibrium probabilities  $P_{eq}$  can be found by solving the rate equation.

Since Eq. (8) is linear with periodic coefficients, there are special solutions of the form [17]

$$\vec{\Psi}[t] = e^{\rho t} \vec{h}[t], \quad (10)$$

where  $\rho$  is constant and the vector  $\vec{h}$  is  $T$  periodic. Since  $\vec{n}$  has  $S$  components, there are typically  $S$  linearly independent solutions  $\vec{\Psi}^{(j)}$  of this special form, corresponding to  $S$  distinct Floquet exponents  $\rho_j$ . In that case, the general solution of Eq. (8) can be written as

$$\vec{n}[t] = \sum_j c_j \vec{\Psi}^{(j)}[t], \quad (11)$$

where the constants  $c_j$  are determined from the initial conditions.

Since our problem has a unique period- $T$  attractor, it follows that exactly one of the Floquet exponents is zero. We label this with the subscript zero so that  $\rho_0=0$ . The attractor gives the equilibrium probabilities

$$P_{eq}[\alpha, t_1] = \Psi_{\alpha}^{(0)}[t_1], \quad (12)$$

where we assume that the function  $\vec{\Psi}^{(0)}$  has been normalized.

Let us suppose we have determined the complete set of Floquet exponents and corresponding normal solutions Eq. (10). Then we can construct the conditional probabilities as follows. Since  $P_c[\beta, t | \alpha, 0]$  is the solution of the rate equation with initial condition

$$n_k[0] = \delta_{k\alpha}, \quad (13)$$

we first determine the constants  $c_{\alpha j}$  such that

$$\sum_j c_{\alpha j} \Psi_k^{(j)}[0] = \delta_{k\alpha}, \quad (14)$$

for  $\alpha=1, \dots, S$ . Then

$$P_c[\beta, t | \alpha, 0] = \sum_j c_{\alpha j} \Psi_{\beta}^{(j)}[t]. \quad (15)$$

Putting this all together yields

$$\langle f[0]f[\tau] \rangle = \sum_{\alpha} \sum_{\beta} f_{\alpha} f_{\beta} \Psi_{\alpha}^{(0)}[0] \sum_j c_{\alpha j} \Psi_{\beta}^{(j)}[\tau] \quad (16)$$

or

$$\langle f[0]f[\tau] \rangle = \sum_j e^{\rho_j \tau} \left( \sum_\alpha \sum_\beta f_\alpha h_\alpha^{(0)}[0] c_{\alpha j} h_\beta^{(j)}[\tau] f_\beta \right). \quad (17)$$

### B. Numerical implementation

To evaluate the last expression, we need to determine the  $\rho_j$ ,  $\vec{h}^{(j)}$ , and  $c_{\alpha j}$  for a given transition matrix  $\mathbf{W}$ . Denote by  $\vec{u}^{(j)}[t]$  the solution to Eq. (8) with initial condition  $\vec{n}(0)$  having all the probability in state  $j$ , namely,  $n_i[0] = \delta_{ij}$ . For each of these  $S$  distinct initial conditions, we numerically integrate Eq. (8) for exactly one period,  $t \in [0, T]$ , at one signal phase  $\varphi$ , and form the  $S \times S$  fundamental matrix  $\Phi[t]$  whose  $j$ th column is  $\vec{u}^{(j)}[t]$  [17]. We then determine the eigenvalues  $\mu_j$  of the *constant* matrix  $\Phi[T]$ , as well as its left and right eigenvectors  $\vec{L}^{(j)}$  and  $\vec{R}^{(j)}$ , respectively. Then

$$\rho_j = \frac{1}{T} \ln \mu_j, \quad (18)$$

$$c_{\alpha j} = \frac{L_\alpha^{(j)}}{\vec{L}^{(j)} \cdot \vec{R}^{(j)}}, \quad (19)$$

and

$$\vec{h}^{(j)}(t) = e^{-\rho_j t} \Phi[t] \cdot \vec{R}^{(j)}. \quad (20)$$

Useful checks on the numerics are that the largest eigenvalue of  $\Phi[T]$  should be exactly 1 (corresponding to the Floquet exponent  $\rho_0=0$  discussed previously); that all of the other eigenvalues satisfy  $\mu_j \in (0, 1)$ ; and that the elements of each column of  $\Phi[t]$  sum to unity for any  $t$ .

Having evaluated Eq. (17), the last step in generating the stationary correlation function is to perform a phase average, by repeating the process for different signal phases; we have found that it is sufficient to average over three equally spaced phases. By the Wiener-Khinchine theorem, the power spectrum is the Fourier transform of the correlation function, which we obtain by sampling the correlation function at a discrete set of points and applying a fast Fourier transform algorithm.

### C. An energy landscape rate model

So far, our description of rate models is fairly general. We now make a particular choice which is directly motivated by the earlier Langevin problem. Corresponding to the  $2^N$  stable fixed points of the (weakly coupled) chain of  $N$  bistable elements, we consider a rate model with  $S=2^N$  states. We choose the coordinates  $\vec{x}_i$  of the  $i$ th state to be the  $i$ th  $N$ -tuple of  $\{c, -c\}$ , where  $c = \sqrt{a/b}$  locates a minimum of the potential energy of an isolated oscillator. (For example, for  $N=2$ , the states are ordered  $\{c, c\}, \{c, -c\}, \{-c, c\}, \{-c, -c\}$ , and the third state  $\vec{x}_3 = \{-c, c\}$  has coordinates  $x_{31} = -c, x_{32} = c$ .)

In choosing the transition rates, we want to exploit the physical intuition available to us from the energy landscape of the Langevin problem. We therefore assume that the transition rates  $W_{ij}$  between initial stable equilibria  $i$  and  $j$  are governed by the potential energy difference  $\Delta U_{ij}$  between

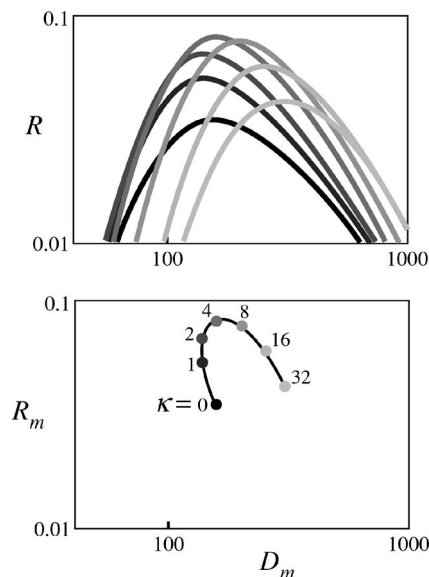


FIG. 5. Rate AESR for  $N=2$ . Upper plot shows the signal-to-noise ratio  $R$  versus noise intensity  $D$  for different coupling strengths  $\kappa$ . Bottom plot focuses on movement of successive maxima, which reveals yet another maximum. Axes have same scales as those in Fig. 3. Same parameters as in Fig. 2.

the initial state and the saddle point linking the two states by an Arrhenius formula

$$W_{ij}[t] = \Gamma e^{-\Delta U_{ij}[t]/D}, \quad (21)$$

where the prefactor  $\Gamma$  carries the units of a rate and  $D$  is noise intensity. For now, we have in mind a situation where the coupling and signal are weak enough that their presence does not radically affect the potential energy landscape; later we will see that this formula works reasonably well even outside the weak-coupling regime. Consequently, we evaluate the potential energy  $U[\vec{x}, t]$  at the *unperturbed* equilibria  $\vec{x}_i$ . For the transition from the  $j$ th to the  $i$ th state,

$$\Delta U_{ij}[t] = U\left[\frac{\vec{x}_i + \vec{x}_j}{2}, t\right] - U[\vec{x}_j, t] \quad (22)$$

for  $i \neq j$ . Together, the last two equations define the off-diagonal elements of  $\mathbf{W}$ . The diagonal elements are determined by probability conservation, which requires that the elements of each column of  $\mathbf{W}$  sum to zero.

### V. COMPARISON

In this section we present results for a few variations of the basic rate model. In all cases they compare reasonably well with each other and also with the earlier Langevin simulations. This suggests that the phenomenon of AESR enjoys a certain robustness. In the next section we turn our attention once more to extracting some deeper understanding of the underlying mechanism involved.

Inspired by the Kramers one-dimensional rate formula, we choose  $\Gamma = a/\pi\sqrt{2}$  in Eq. (21). Then, for the finite-state transition rate model for  $N=2$ , Fig. 5 plots signal-to-noise ratio  $R$  versus noise intensity  $D$  for various coupling

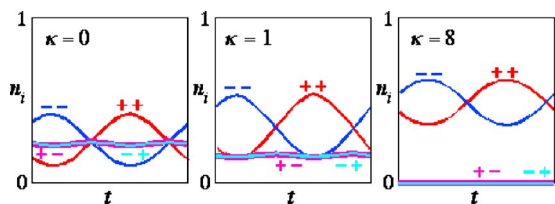


FIG. 6. (Color online) Time variation of the state occupation probabilities for  $N=2$  as a function of coupling  $\kappa$ . Consistent with the vanishing of the asymmetric minima of the underlying potential energy landscape, the asymmetric states  $+-$  and  $-+$  become depopulated at large coupling.

strengths  $\kappa$ . As coupling increases, the maximum  $R$  increases and then decreases, generating a maximum within a maximum, as in the Langevin model of Fig. 3.

Figure 6 plots the time variation of the probabilities  $n_i[t]$  for three different couplings  $\kappa$ . For large coupling, the occupation probability of the asymmetric states,  $+-$  and  $-+$ , which are always equal by symmetry, empty (as the transition rates from these states diverge exponentially). This is consistent with the vanishing of the corresponding minima in the underlying potential energy landscape of the corresponding Langevin problem. The asymmetric states become depopulated at large coupling, when large wavelength modes dominate the array dynamics, and the population of the symmetric states oscillates sinusoidally with the signal.

Figure 7 compares the change in the signal-to-noise maxima as a function of coupling  $\kappa$  for the Langevin and rate

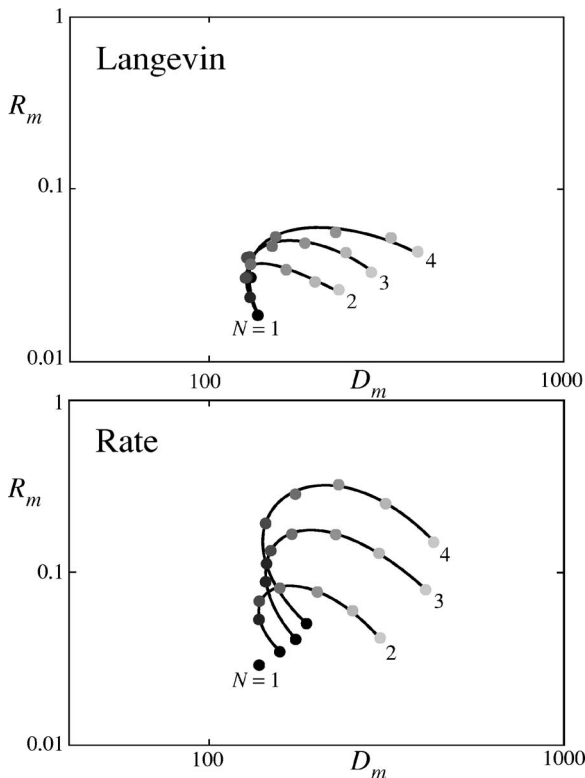


FIG. 7. Comparison of Langevin and finite-state transition rate model of AESR for arrays of length  $N=1, 2, 3, 4$  at the parameters of Fig. 2.

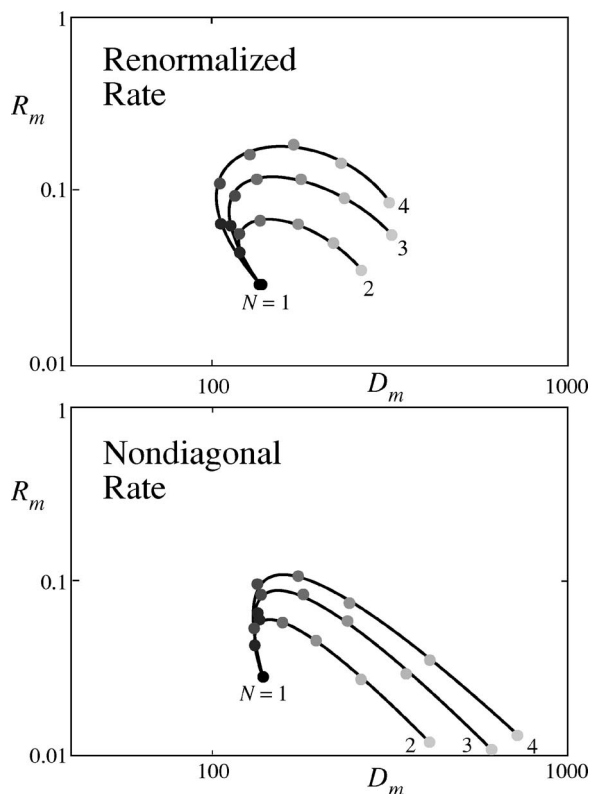


FIG. 8. Comparison of modified finite-state transition rate models at the parameters of Fig. 2.

models for arrays of size  $N=1, 2, 3, 4$ . In each case, we focus on the middle oscillator. Qualitative agreement is very good. However, the rate model lacks a common uncoupled  $\kappa=0$  limit. For the Langevin model, curves of constant  $N$  are anchored to the coupling-independent  $N=1$  point, but for the rate model, curves of constant  $N$  drift to larger maximum signal-to-noise ratio  $R$  and noise intensity  $D$ . The rate model can be readily renormalized to correct for this (by scaling the prefactor and the noise intensity, for example).

Alternately, a simpler rate model allowing only nondiagonal transitions, wherein only one coordinates changes during each transition, naturally exhibits a common uncoupled limit. We obtain this rate model from the previous one by zeroing all elements of the rate matrix  $W$  corresponding to transitions in which more than one coordinate changes. (The resulting  $W$  is a sparse, banded matrix with nonzero entries along main diagonals beginning with columns  $2^n$ , where  $n=0, 1, 2, \dots, N-1$ . This suggests possible numerical advantages.) The nondiagonal rate model's large coupling behavior is not as good as its small coupling behavior, because diagonal transitions dominate at high coupling where long wavelength modes dominate the corresponding Langevin model. Nevertheless, the nondiagonal rate model is also in qualitative agreement with the Langevin model, including—and most importantly—exhibiting a local maximum signal-to-noise ratio in both noise *and* coupling. Figure 8 compares these improved rate models with the same scales of Fig. 7.

If the coupling  $\kappa$  is small, the potential energy landscape is similar to the unperturbed landscape  $U_0[\vec{x}]$ , and power

series expansions provide good approximations to the locations of the perturbed extrema. Generalizing Eq. (21) to

$$W_{ij} = \Gamma_{ij} e^{-\Delta U_{ij}/D}, \quad (23)$$

$$\mathbf{W} = \begin{pmatrix} 1 - 2W_{1,1} & W_{1,-1} & W_{1,-1} & 0 \\ W_{1,1} & 1 - W_{1,-1} - W_{-1,1} & 0 & W_{-1,-1} \\ W_{1,1} & 0 & 1 - W_{1,-1} - W_{-1,1} & W_{-1,-1} \\ 0 & W_{-1,1} & W_{-1,1} & 1 - 2W_{-1,-1} \end{pmatrix}, \quad (24)$$

where

$$\Gamma_{ij} = \frac{\sqrt{(a-\kappa)[2(a-\kappa) + 3ij\kappa]}}{2\pi} \quad (25)$$

and

$$\Delta U_{ij} = \frac{(a-\kappa)^2}{4b} + ij \frac{\kappa(a-\kappa)}{b} + j \left| -jc - i \frac{3\kappa}{2b\tilde{c}} \right| A \cos[\omega_s t + \phi_0] \quad (26)$$

with

$$\tilde{c} = \sqrt{\frac{a-\kappa}{b}}. \quad (27)$$

For small to moderate coupling  $\kappa$ , these equations imply AESR qualitatively similar to that of the nondiagonal rate model of Fig. 8.

## VI. DISCUSSION AND HEURISTICS RECONSIDERED

Our finite-state transition rate models of AESR nicely capture the qualitative features of the corresponding Langevin models. They are intuitive and easy to construct and are fast to implement, at least for small arrays. They should facilitate the study of the effects of parameters, especially  $a$  and  $b$  for the bistable potential wells and  $\epsilon$  and  $f$  for the signal, on AESR. Unlike the Langevin models, it is easy to efficiently tune and run the transition rate models with the signal just barely above the noise, and so investigate important marginal situations of AESR. Furthermore, the Floquet theory formulation can be used as a springboard for developing an analytic theory of AESR [2,19].

While it is encouraging to have found a rate description which agrees reasonably well with the Langevin model, we can ask if it leads us to a better physical understanding of AESR. In fact, the combination of the transition rate formulation and the energy landscape model gives us the means to make concrete our earlier heuristic picture, as we now show.

Consider once again the  $N=2$  situation, and focus on the transition between the  $--$  and  $++$  states. The total rate

and approximately evaluating the potential energy  $U[\vec{x}, t]$  at the perturbed equilibria, we can explicitly write the transition rate matrix for any  $N$ . For an  $N=2$  array with free ends we find

is a sum over all paths (all transition sequences) between the  $--$  and  $++$  states. We include only the simplest ones, those involving one and two steps, since typically the more transitions within a path the smaller its contribution to the overall rate. Figure 9 indicates the three simplest paths. Path B is the direct path, while paths A and C represent transitions where first one, then the other, particle switches. The total rate is the sum of the three individual rates

$$W = W_A + W_B + W_C. \quad (28)$$

Path A is itself a two-step process. If we assume the steps are statistically independent and occur sequentially

$$\frac{1}{W_A} = \frac{1}{W_1} + \frac{1}{W_2}, \quad (29)$$

where  $W_1$  is the rate for the first step, and  $W_2$  for the second. By symmetry,  $W_C = W_A$ . Putting this all together, we have

$$W = \frac{2}{1/W_1 + 1/W_2} + W_B. \quad (30)$$

The energy landscape model gives us a way to directly evaluate these rates. The energy barrier between the  $--$  and

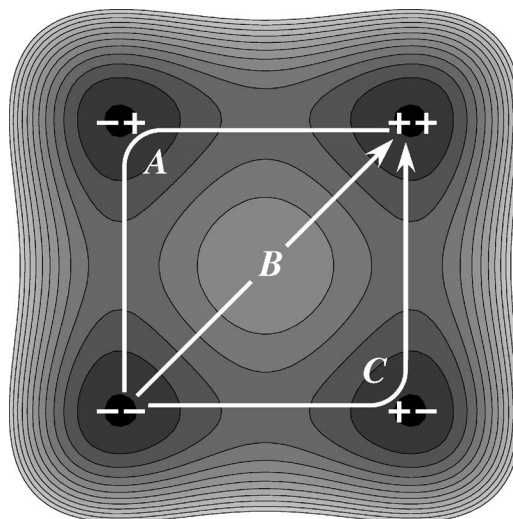


FIG. 9. Simplest paths between the  $--$  and  $++$  states.

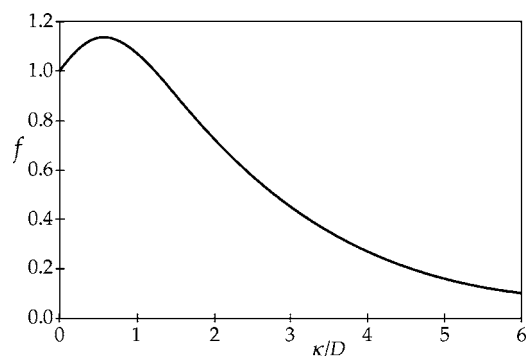


FIG. 10. Indirect rate coupling factor  $f$  exhibits a local maximum as a function of coupling strength  $\kappa$ .

$-+$  states is the sum of the double-well, spring, and signal energy differences [see Eq. (2)]

$$\Delta + \frac{1}{2}\kappa + \epsilon \cos \omega t. \quad (31)$$

This is the energy difference between the saddle point and the stable fixed point (taking “unperturbed” values for the coordinate positions  $-1, 0, +1$ ). The energy barrier between  $-+$  and  $++$  states is

$$\Delta - \frac{3}{2}\kappa + \epsilon \cos \omega t, \quad (32)$$

where the factor of 3 arises from the fact that the spring energy is four times greater in the  $-+$  state than at the saddle point separating it from the  $++$  state. Finally, the energy barrier for a direct transition between  $--$  and  $++$  states is

$$2\Delta + 2\epsilon \cos \omega t. \quad (33)$$

Using the Arrhenius-type formula  $W \sim \exp[-U/D]$  to convert energy barriers into rates, we find

$$W = \exp\left(-\frac{\Delta + \epsilon \cos \omega t}{D}\right) f[\kappa] + \exp\left(-\frac{2\Delta + 2\epsilon \cos \omega t}{D}\right), \quad (34)$$

where

$$f[\kappa] = \frac{2}{\exp(\kappa/2D) + \exp(-3\kappa/2D)}. \quad (35)$$

The last term in Eq. (34) is the direct rate, and (of course) does not depend on the coupling parameter  $\kappa$ . The effect of coupling on the indirect rate is carried by the factor  $f[\kappa]$ .

In Fig. 10, we plot  $f$  vs  $\kappa/D$ . In the uncoupled limit,  $f \rightarrow 1$ , and the indirect rate dominates over the direct rate (as it should). For small coupling,  $f$  increases, and the indirect rate is enhanced. For large coupling (and fixed noise level  $D$ ),  $f \sim \exp[-\kappa/2D]$  and the direct rate eventually dominates over

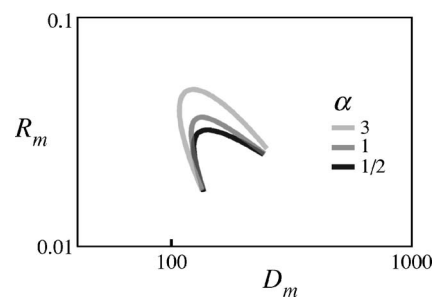


FIG. 11. Superlinear coupling ( $\alpha=3$ ) produces greater enhancement than sublinear coupling ( $\alpha=1/2$ ). The curves are smooth fits to the numerical data.

the indirect rate. These features agree with what we observe in our simulations.

We are thus led to the following interpretation and (see below) a testable prediction. In the first step along the indirect path, the presence of coupling costs the system energy, and this *suppresses* transitions; however, *for small coupling* the second step more than compensates for this cost, leading to an overall enhancement of the transition rate. In terms of the energy landscape, the presence of the spring makes it more difficult for any one particle to surmount its potential barrier, but once over the barrier the deterministic dynamics drives the system to the  $+ -$  fixed point, putting additional energy into the spring, which makes it “extra favorable” for the other particle to follow along. But for enhancement of the overall rate it is not enough that the coupling force is attractive: from Eq. (29), we see that if the suppression of the first step is larger than a factor of 2, the total rate is necessarily lower no matter how great the enhancement of the second step.

These considerations are intended to provide a rough estimate of the situation. That said, if we follow through the full implications, we are led to a testable prediction. Referring to Eq. (32), we note that if the numerical factor of 3 was instead smaller than unity, the coupling factor  $f$  would be monotonically decreasing and the predicted optimal coupling would be zero, even if the coupling was attractive. Conversely, larger values of this numerical factor should enhance AESR. We have tested this by simulating the Langevin problem with a coupling force of  $\text{sgn}[x_2 - x_1]\kappa|x_2 - x_1|^\alpha$  for various values of the parameter  $\alpha$ . We expect superlinear coupling  $\alpha > 1$  to enhance AESR and sublinear coupling  $\alpha < 1$  to diminish AESR. As shown in Fig. 11, numerical simulations support these expectations.

#### ACKNOWLEDGMENTS

J.F.L. thanks The College of Wooster for making possible his sabbatical at Georgia Tech. This work was supported in part by ONR Grant No. N00014-99-1-0592.

- [1] R. Benzi, A. Sutura, and A. Vulpiani, *J. Phys. A* **14**, L453 (1981).
- [2] L. Gammaitoni, P. Hänggi, P. Jung, and F. Marchesoni, *Rev. Mod. Phys.* **70**, 223 (1998).
- [3] P. Jung, U. Behn, E. Pantazelou, and F. Moss, *Phys. Rev. A* **46**, R1709 (1992).
- [4] J. F. Lindner *et al.*, *Phys. Rev. Lett.* **75**, 3 (1995).
- [5] J. F. Lindner *et al.*, *Phys. Rev. E* **53**, 2081 (1996).
- [6] F. Marchesoni, L. Gammaitoni, and A. R. Bulsara, *Phys. Rev. Lett.* **76**, 2609 (1996).
- [7] T. Kanamaru, T. Horita, and Y. Okabe, *Phys. Rev. E* **64**, 031908 (2001).
- [8] M. Löcher, G. A. Johnson, and E. R. Hunt, *Phys. Rev. Lett.* **77**, 4698 (1996).
- [9] M. Löcher *et al.*, *Chaos* **8**, 604 (1998).
- [10] A. C. H. Rowe and P. Etchegoin, *Phys. Rev. E* **64**, 031106 (2001).
- [11] J. P. Sharpe *et al.*, *Phys. Rev. E* **67**, 056222 (2003).
- [12] A. Neiman and L. Schimansky-Geier, *Phys. Lett. A* **197**, 379 (1995).
- [13] U. Siewert and L. Schimansky-Geier, *Phys. Rev. E* **58**, 2843 (1998).
- [14] R. Rozenfeld and L. Schimansky-Geier, *Chaos, Solitons Fractals* **11**, 1937 (2000).
- [15] B. McNamara and K. Wiesenfeld, *Phys. Rev. A* **39**, 4854 (1989).
- [16] P. E. Kloeden and E. Platen, *Numerical Solutions of Stochastic Differential Equations* (Springer, Berlin, 1992).
- [17] D. W. Jordan and P. Smith, *Nonlinear Ordinary Differential Equations: An Introduction to Dynamical Systems* (Oxford University Press, New York, 1999).
- [18] P. Hänggi, P. Talkner, and M. Borkovec, *Rev. Mod. Phys.* **62**, 251 (1990).
- [19] K. Wiesenfeld *et al.* (unpublished).